Int J Adv Manuf Technol (2011) 52:263–278
DOI 10.1007/s00170-010-2720-5

ORIGINAL ARTICLE

Development of friction identification methods for feed drives of CNC machine tools

Syh-Shiuh Yeh · Hsin-Chun Su

Received: 18 January 2010 / Accepted: 5 May 2010 / Published online: 20 May 2010

Abstract Friction exists in the feed drive servomechanisms of CNC machine tools and usually affects their motion. Although many experiments have been performed to identify the friction characteristics of a feed drive servomechanism, problems such as unmodeled dynamics and position-dependent perturbations still exist and significantly affect the friction identification results. In this study, in order to obtain reliable friction and velocity data values, a modified velocity control system is developed to reduce the effects induced by unmodeled dynamics, and a friction extraction method is developed to remove the adverse effects of position-dependent perturbations. Furthermore, several experiments and motion tests are carried out on a three-axis CNC milling machine to demonstrate the feasibility of the proposed friction identification method. The experimental results indicate that the friction-compensated motion control system with the friction model obtained in this study reduces the root mean square value of tracking errors by 44.16%. Moreover, as compared to a conventional identification method, the root mean square value of tracking errors is found to further reduce by 9.52% in the experiments.

Keywords Friction · Identification · Feed drive · CNC · Machine tool

S.-S. Yeh (✉)
Department of Mechanical Engineering,
National Taipei University of Technology,
Taipei 10608, Taiwan
e-mail: ssyeh@ntut.edu.tw

H.-C. Su
Mechanical and Systems Laboratories,
Industrial Technology Research Institute,
Hsinchu 310, Taiwan

1 Introduction

Friction is a physical phenomenon that occurs in mechanical systems and usually exerts some adverse effects on their motions, such as steady-state errors, stick-slip oscillations, and poor tracking and contouring performances. In order to mitigate these adverse effects and achieve high-precision motions, model-based friction compensators are usually used in the design of motion control systems for compensating the friction phenomenon [1–7]. Therefore, good friction models are required for motion control design, and the compensation performance heavily depends on the accuracy of the applied friction models.

A good friction model is usually developed on the basis of the knowledge of the friction behaviors of a mechanical system. However, it is difficult to model friction because there are many factors affecting the friction behavior, such as the material, lubrication, and surface texture of the bodies in contact [8–15]. Thus far, many simplified friction models have been proposed for motion control and compensation design [3, 4, 8, 15, 16]. An identification process, usually based on an optimization method, is applied to identify the parameters of friction models. For instance, Cheok et al. [17] used the simplex method to determine the parameters of the Karnopp friction model [18]. Kim et al. [19] proposed an acceleration evolutionary programming method, which is an experimental identification method, to identify the parameters of the seven-parameter friction model presented by Armstrong-Helouvry et al. [4]. For the given friction–velocity map obtained experimentally, Canudas-de-Wit and Lischinsky [20] also used the simplex method to obtain the optimal parameters of the LuGre friction model [21].

Conventionally, two experiments, a breakaway experiment and a constant velocity experiment, are performed to obtain

friction and velocity data values used by the identification processes of friction models [15, 20, 22]. The breakaway experiment involves allowing the moving part of a mechanical system to come to rest at certain positions, ramping up the driving torque and measuring the torque required to initiate the motion of the moving part. Therefore, the breakaway experiment, which involves sampling the static friction at a suitable spatial frequency, can be performed to identify static friction and develop a friction compensation lookup table for determining compensation. Furthermore, the constant velocity experiment can be carried out to identify the velocity-dependent friction in a mechanical system by constructing a friction–velocity map from the measurements performed during the constant velocity motions of a moving part. Linear or nonlinear optimization algorithms are then used to identify the parameters of a friction model by fitting the data to the friction–velocity map obtained. Although the current experimental methods can be employed to obtain data values for friction identification processes, some problems still exist, which can significantly affect the identification results. Since considerable position-dependent perturbations exist in mechanical systems, usually caused by the surface irregularities, assembly errors, and geometric machining errors of mechanical parts, the velocity responses are always perturbed and can deteriorate the obtained friction–velocity map. In addition, unmodeled dynamics, usually induced by several flexible and inertia elements in a mechanical system, increase the uncertainties in the estimated friction characteristics.

The disturbance observer (DOB), introduced by Ohnishi [23], is usually applied to motion control systems in order to compensate for the external disturbances and to reduce the adverse effects induced by system uncertainties and nonlinearities. In this study, considering the merits of DOB feedback control [23], the DOB structure is integrated into a velocity control loop to compensate for the speed perturbations induced by external disturbances and system uncertainties. Moreover, since the position-dependent perturbations are invariant under fixed mechanical conditions, a friction extraction method is developed to remove position-dependent perturbations; the method involves the subtraction of different torque values measured at the same positions of the moving part. The friction and velocity data values, obtained by using the modified velocity control loop and applying the developed friction extraction method, can be applied to identify the parameters of a given friction model so that the friction model can thereby reduce the uncertainties in the estimated friction characteristics. Furthermore, several experiments and motion tests are carried out on a three-axis CNC milling machine in order to demonstrate the feasibility of the approaches proposed in this study.

This paper is organized as follows. Section 2 describes the experiment design and measurement method used in this study in order to obtain data values for identifying the parameters of a given friction model. Section 3 proposes identification methods and reports the obtained identification results in detail. Section 4 presents the experimental results of motion tests in order to demonstrate the feasibility of the friction identification methods proposed in this study. Finally, Section 5 concludes this study.

2 Experiment design and measurement

2.1 Experimental setup

Experimental studies were made on a three-axis CNC milling machine comprising an industrial PC, a digital signal processor (DSP)-based motion control card, and a mechanical system equipped with commercial servomotor packs. Figures 1 and 2 show a schematic drawing and a photograph of the experimental setup, respectively. An industrial PC with a Pentium IV 2.8-GHz CPU is used to provide functions and includes an interface for human and machine operations, implementation of identification methods, and recording data values during experiments. The DSP-based motion control card with a high-performance TI TMS320F2812 DSP is used as the interface for sending motion commands to, and receiving feedback signals from, the servomotor packs with a sampling period of 1.0 ms. The mechanical system of the milling machine is mainly composed of a vertical axis and biaxial moving table. The vertical axis with a rotary spindle can vertically move a cutting tool so as to perform machining with different depths. The biaxial moving table, which is the main object of this study, is driven by two Panasonic A4-type AC servomotor packs [24] equipped with built-in velocity and torque control loops. Here, torque and velocity command signals are sent to each amplifier of the servomotor packs through a 12-bit D/A converter installed on the DSP-based motion control card. A rotary incremental encoder is directly coupled to the motor of a servomotor pack, and the generated encoder signals, used to indicate the angular positions of the motor, are received through a 32-bit decoder implemented on the DSP-based motion control card. Furthermore, an angular velocity signal is computed by differentiating the angular position over a sampling period. A 12-bit A/D converter implemented on the DSP-based motion control card is used to receive analog signals from the servomotor packs in order to obtain the torque values that actuate the biaxial moving table. MATLAB software is used to facilitate the development of identification and control algorithms.

The biaxial moving table mainly consists of a moving part and two feed drive servomechanisms, as shown in

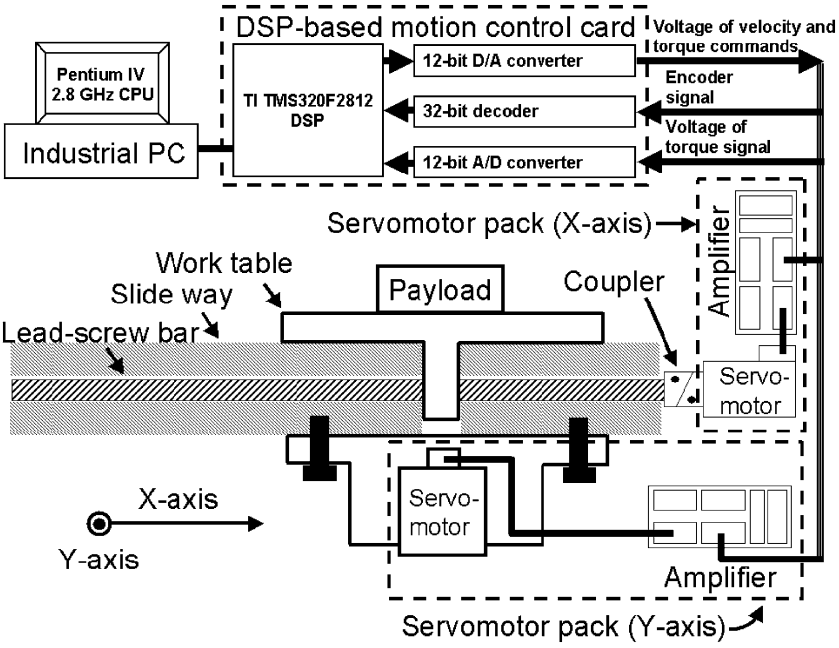

Fig. 1 Schematic drawing of the experimental setup

Figs. 1 and 2. The *X*-axis along with the moving part (it is also the worktable as shown in Fig. 2) is installed on the *Y*-axis. Here, the moving part, which is placed on a slide way, is driven by a servomotor pack through a coupler, lead-screw bar, and nut. The moving part and the support rails of the slide way are both made of cast iron. Therefore, lubrication must be guaranteed before performing the experiments. Grease has been used as a lubricant in the experimental studies. Table 1 lists some specifications of the main components used in this study.

2.2 Measurement and control

Friction and velocity data measurements were performed during the motions of the moving part placed on each feed drive servomechanism of the CNC milling machine. Figure 3 schematically shows the motion of the moving part, i.e., the worktable, during the experiments in this study. The moving part starts to move forward from return position A, sequentially passes through the home position and target position, and reaches return position B; then, it starts to move

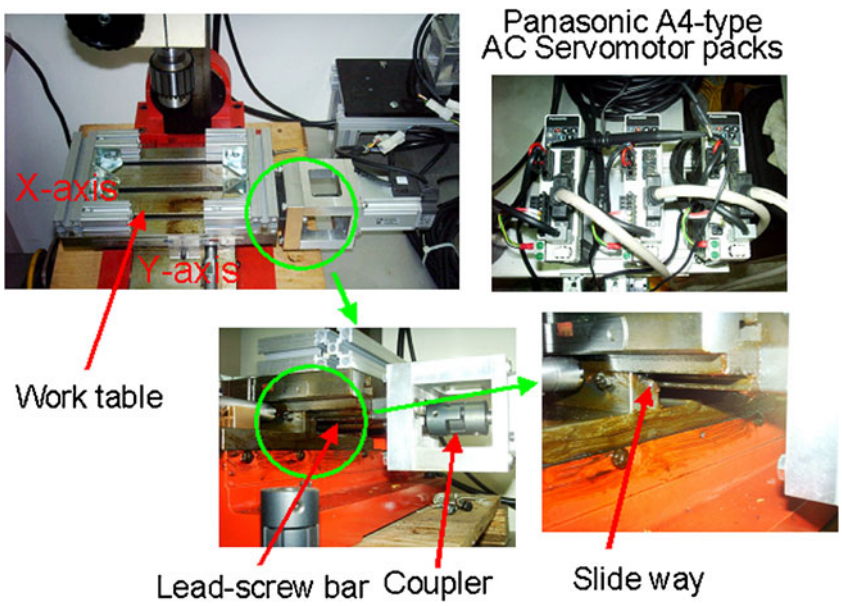

Fig. 2 Photograph of the experimental setup

Table 1 Specifications of main components in this study

Milling machine	Worktable area (mm×mm)	240×145
	Size (mm×mm×mm)	500×350×690
	X/*Y*/*Z* stroke (mm×mm×mm)	130×180×230
	Maximum speed (mm/min)	1,200
	Screw lead (mm)	1.2
Servomotor pack	Rated power (kW)	0.2
	Rated torque (Nm)	0.64
	Maximum torque (Nm)	1.9
	Rated angular velocity (rpm)	3,000
	Maximum angular velocity (rpm)	5,000
	Inertia of rotor (kg m^2)	0.42×10^{-4}
	Resolution of encoder (encoder increments/revolution)	10,000
	Resolution of encoder (radian/encoder increment)	6.2832×10^{-4}

backward from return position B and reaches return position A. In each experiment, the moving part moved along the motion path and undertook several forward and backward motions with different motion velocities. Here, it should be noted that the motion path between return position A and the home position and that between return position B and the target position must be sufficiently long in order to ensure steady-state and backlash-free motions between the home and target positions. Therefore, the identification results were valid when the moving part moved within the path between the home and target positions. Furthermore, in this study, the positions of the moving part were represented by the encoder increments obtained from a rotary encoder coupled to the motor of the servomotor pack used. The home position was determined by using a zero encoder increment, and the target position was located at 150,000 encoder increments. In each experiment, the cyclic motions between return positions A and B were performed several times so as to obtain the average behavior of friction. Furthermore, an infrared thermometer was employed to measure the temperature around the moving table, and the temperature was controlled within the range of 28°C to 29°C during all of the experiments. The industrial PC recorded data values with a period of 10 ms, and the acquired data included the motion direction, angular position, velocity, acceleration of the driving motor, torque value that actuated the tested feed drive servomechanism, and motion time. The units of the acquired position, velocity, and acceleration signals were encoder increments, radian per second, and radian per square second, respectively; the unit of the acquired torque value was newton meter. Usually, a large number of data points are required to obtain good identification results, and therefore, a long period of experimentation is mandatory.

Figure 4 shows the modified velocity feedback control structure composed of a built-in velocity feedback control loop and a disturbance observer. Each of the applied servomotor packs provided a built-in velocity control loop, and the velocity controller generated actuating torque τ_m to overcome external torque τ_{ext} and actuate a feed drive servomechanism with equivalent inertia J_a. ω_{cmd} and ω denote the angular velocity command and the corresponding angular velocity response, respectively. Here, the velocity controller was tuned using the built-in auto-tuning function

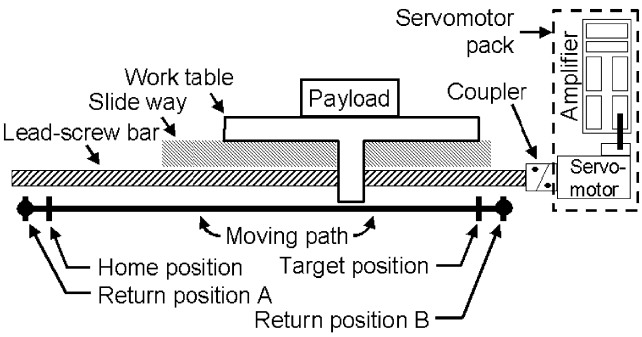

Fig. 3 Motion of the moving part (worktable) placed on a feed drive servomechanism

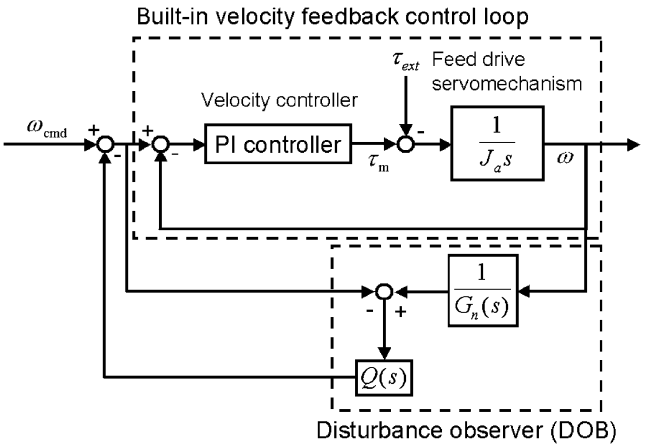

Fig. 4 Modified velocity feedback control structure used in this study

[24] in order to enable the feed drive servomechanism to achieve good velocity tracking results. Moreover, a DOB was integrated into the built-in velocity control loop in order to reduce the adverse effects of uncertainties and nonlinearities in the feed drive servomechanism used. Here, $G_n(s)$ represents the nominal plant model of the built-in velocity control loop, which could be obtained by identification methods [25]. $Q(s)$ denotes a low-pass filter used in the DOB feedback loop for disturbance compensation. The design of $Q(s)$ is the most important consideration because it significantly affects the stability and execution performance of DOB feedback control systems and has therefore been discussed in several papers [26–28]. In this study, a simple first-order low-pass filter was considered because of its simple implementation. The bandwidth of the filter was tuned manually so as to mitigate the effects of disturbances containing high-frequency components and to maintain the stability of the DOB feedback control system used.

Two experiments, a breakaway experiment [15, 22] and a constant velocity experiment [15, 20], were performed on the three-axis CNC milling machine shown in Figs. 1 and 2.

2.3 Breakaway experiment

In this study, breakaway experiments, each with several test periods, were carried out as follows. First, before conducting a breakaway experiment, the servomotor pack intended to be used in the experiment was switched to the velocity control loop, and then, the tested feed drive servomechanism was "warmed up" by moving the worktable throughout the workspace for a minute prior to collecting test data in order to eliminate the influence of the dwell time effect [15]. After the warm-up procedure, the servomotor pack was set to the torque control loop such that torque commands could be directly given to actuate the tested feed drive servomechanism. Second, the moving part of the tested feed drive servomechanism was positioned at a starting point, and then, the torque command was gradually increased until the motor output torque was sufficient to overcome the static friction of the tested feed drive servomechanism. Here, the torque command was increased from zero by sequentially adding step commands with a magnitude of 0.002 Nm/s. The motor output torque could be obtained from the interface signal of the amplifier of the applied servomotor pack [24]. As soon as the motor output torque overcame the static friction, the moving part moved; then, the applied torque command was reduced to zero and the moving part was allowed to come to rest. The starting position (the position where the moving part started its motion) and the breakaway torque (the motor output torque that overcame the static friction) were recorded during this test period. After the moving part came to rest, a new test period was initiated.

In this study, many test periods were used in a breakaway experiment. Moreover, ten breakaway experiments, each with motions in the positive direction (from the home position to the target position) and negative direction (from the target position to the home position), were conducted to obtain the average friction behavior. In addition, the method proposed by Karnopp [18] was employed to obtain the breakaway torque in a test period.

2.4 Constant velocity experiment

A constant velocity experiment was performed to obtain friction and velocity data values during constant velocity motions of a tested feed drive servomechanism in order to construct a friction–velocity map for the estimation of velocity-dependent frictions. Similar to a breakaway experiment, the servomotor pack used was switched to the velocity control loop, and then, a warm-up procedure was performed on the tested feed drive servomechanism before conducting the constant velocity experiment. Here, the modified velocity feedback control structure, as shown in Fig. 4, was used. The bandwidth of the modified velocity feedback control loop was 14.02 Hz.

In a constant velocity experiment, the moving part of the tested feed drive servomechanism was positioned at return position A, and then a positive step velocity command was given to the modified velocity feedback control loop such that the moving part moved to return position B at a constant velocity. Thereafter, a negative velocity step command with the same magnitude was applied to actuate the moving part so that it returned to return position A. Ten test periods were used for a given step velocity command in order to obtain average data values, and 13 step velocity commands with different levels ranging from 0.1571 to 104.7198 rad/s were given in order to obtain torque and velocity data values for constructing a friction–velocity map. In this study, ten constant velocity experiments were conducted in order to obtain the average behavior of friction.

3 Friction identification methods and results

3.1 Identification of static friction

In this study, a breakaway experiment was conducted to identify the static friction of the X-axis feed drive servomechanism, and the experimental results are shown in Fig. 5. Here, the average values of the measured data are shown and used for analysis because they represent the repeatable part of the measured data and reduce the adverse effects of measurement noises. In order to investigate the positional dependency of the friction, friction-versus-

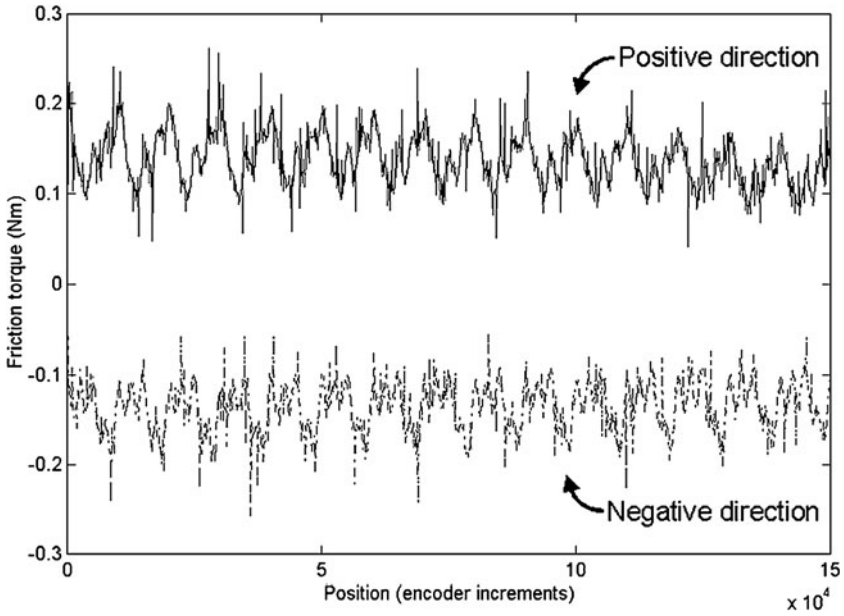

Fig. 5 Identified static friction in two directions

position curves were plotted for both the positive and negative directions, as shown in Fig. 5. These curves were found to fluctuate significantly depending on the angular position of the motor shaft, and thus, the identified friction is clearly position-dependent. Moreover, because the alignment imperfections in transmission systems generally induce oscillating frictions, the static friction exhibits oscillations with different frequencies. Although the friction-versus-position curves obtained for both positive and negative directions exhibit similar average friction, the curve patterns are different because of the asymmetry effect of friction [15]. In general, standard deviation is used to indicate the repeatability of the identified static friction [15]. In this study, the average values of the standard deviation were 0.0055 and 0.0062 Nm for the positive and negative directions, respectively, which were lower than 5% of the corresponding average values.

In this study, spectral analysis using a fast Fourier transformation (FFT) algorithm [29] was applied to analyze the frequency characteristics of the identified static friction. Figure 6 shows the FFT results for the identified static friction shown in Fig. 5. Here, the magnitude of each FFT component is normalized in order to show the percentage of the FFT component with respect to the average friction and

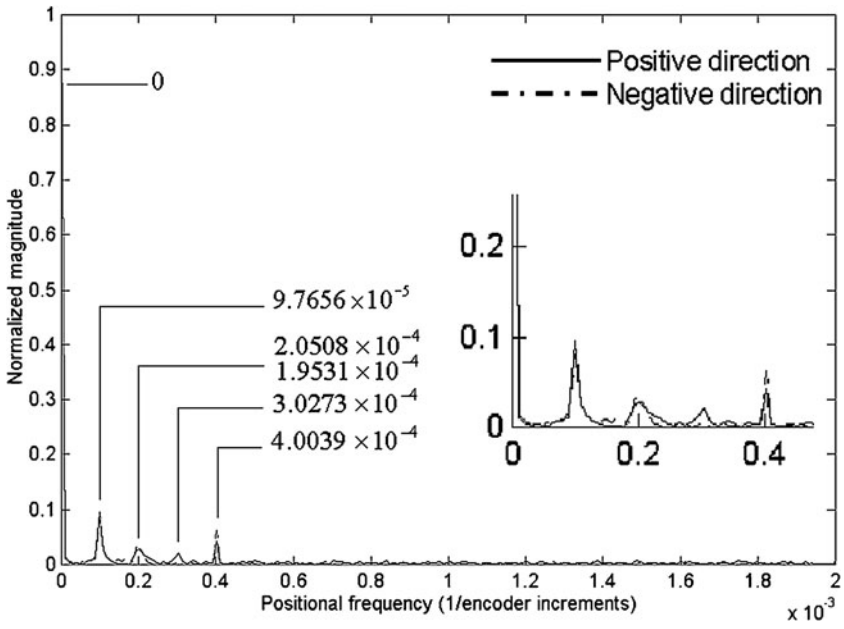

Fig. 6 FFT results for the identified static friction

to indicate the significance of the FFT component. A larger normalized magnitude for an FFT component indicates that the FFT component is more significant. Here, the basic positional frequency used in the FFT analysis was 0.01 (encoder increments)$^{-1}$; this value implies that the static friction was sampled with a sampling period of 100 encoder increments. More refined FFT results can be obtained as the basic positional frequency becomes higher, that is, as the experimentation time becomes longer. However, in this study, the basic positional frequency was set to 0.01 (encoder increments)$^{-1}$ because the significant FFT components were observed identically even though the basic positional frequency was higher than 0.01 (encoder increments)$^{-1}$. Here, the FFT components with normalized magnitudes larger than 0.02 (2% of the average value of the static friction) were considered to be significant FFT components. Note that the FFT components were functions of the reciprocal values of the positional increments. For instance, the FFT component with a positional frequency of $1/(1.0240\times10^4)$ corresponded to a repeatable and periodic friction with a positional period of 1.0240×10^4 encoder increments; in other words, the friction repeated itself every 1.0240×10^4 encoder increments. Table 2 lists the significant FFT components shown in Fig. 6. The FFT component with a positional frequency of 0 (encoder increments)$^{-1}$ represents the average static friction of the tested feed drive servomechanism. Since one revolution of the motor shaft generated 10,000 encoder increments, the FFT component with a positional frequency of approximately 9.7656×10^{-5} (encoder increments)$^{-1}$ can be considered to be the static friction induced by the interaction among the motor shaft, coupler, lead-screw bar, and nut in the tested feed drive servomechanism. The other significant components were close to the harmonic frequencies of the 9.7656×10^{-5} (encoder increments)$^{-1}$ frequency. Hence, these other significant FFT components can also be considered to arise from the interaction of the mechanical parts in the transmission system. The other FFT components could be considered to be the static friction resulting from the interaction between the moving part and the support rails of the slide way used in the tested feed drive servomechanism. Usually, it is difficult to identify the sources of these other FFT components because they are significantly affected by the surface textures of the moving part and the support rails. Moreover, different manufacturing processes usually generate different surface textures for machined parts. Mechanical parts with small and regularly distributed surface structures could cause FFT components with normalized magnitudes of <0.02. In addition, the random friction component also exists because of the establishment and breaking of asperity contacts between sliding surfaces [22].

Table 2 Significant components of the FFT analysis

No.	Positional frequency ((encoder increments)$^{-1}$)	Positional period (encoder increments)	Normalized magnitude
Positive direction			
1	0	–	1
2	9.7656×10^{-5}	1.0240×10^{4}	9.6094×10^{-2}
3	2.0508×10^{-4}	4.8762×10^{3}	2.9107×10^{-2}
4	3.0273×10^{-4}	3.3032×10^{3}	2.1176×10^{-2}
5	4.0039×10^{-4}	2.4976×10^{3}	4.2183×10^{-2}
Negative direction			
1	0	–	1
2	9.7656×10^{-5}	1.0240×10^{4}	8.3959×10^{-2}
3	1.9531×10^{-4}	5.120×10^{3}	3.5844×10^{-2}
4	–	–	–
5	4.0039×10^{-4}	2.4976×10^{3}	6.4360×10^{-2}

The identified static friction, which contains small and random friction components, as shown in Figs. 5 and 6, cannot be directly applied to develop a friction compensation lookup table. Therefore, in this study, a low-pass filter is applied to filter out the random friction components. In order to preserve the significant components listed in Table 2, the low-pass filter was designed to have a bandwidth of 0.0005 (encoder increments)$^{-1}$. Figure 7 shows the filtered static friction curves for both the positive and negative directions. This figure also shows the difference between the filtered and the identified static friction curves. For the difference in the positive direction, the calculated average value is 2.1239×10^{-4}Nm and the standard deviation is 1.3238×10^{-2}Nm. For the difference in the negative direction, the calculated average value is -1.8010×10^{-4}Nm and the standard deviation is 1.2479×10^{-2}Nm. The differences in both cases have average values almost equal to zero, and the standard deviations in both cases are lower than 10% of the corresponding average values. From these results, we can say that it is feasible to use filtered static friction curves for developing friction compensation lookup tables.

3.2 Identification of velocity-dependent friction

In this study, a constant velocity experiment was carried out to obtain friction and velocity data in order to construct a friction–velocity map for the identification of the velocity-dependent friction of the *X*-axis feed drive servomechanism. Consider a feed drive servomechanism actuated by a motor with the following equation of motion:

$$\tau_m - \tau_f = J_a\dot{\omega} = J_a\ddot{\theta} \tag{1}$$

where J_a denotes the equivalent inertia of the feed drive servomechanism; θ and ω denote the angular position and angular velocity of the motor shaft, respectively; $\dot{\omega}$ and $\ddot{\theta}$

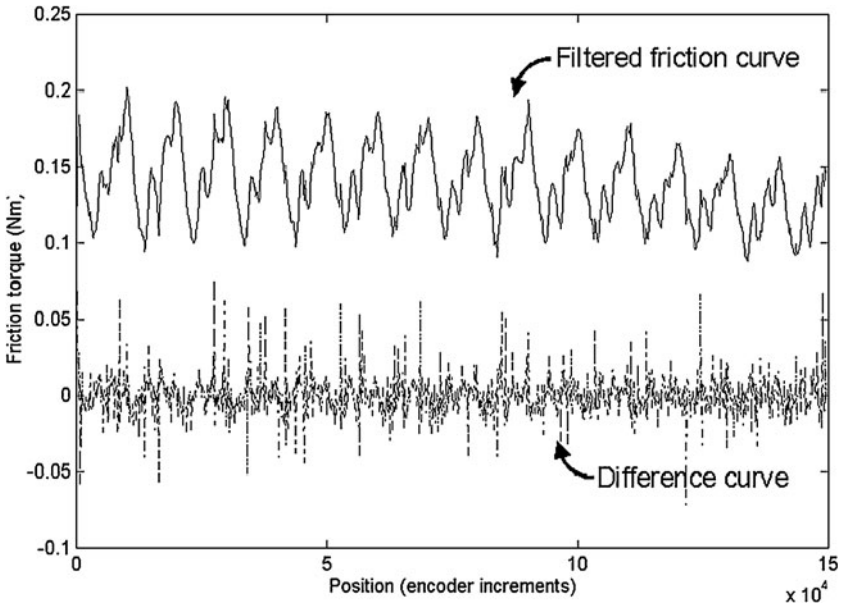

(a) Positive direction

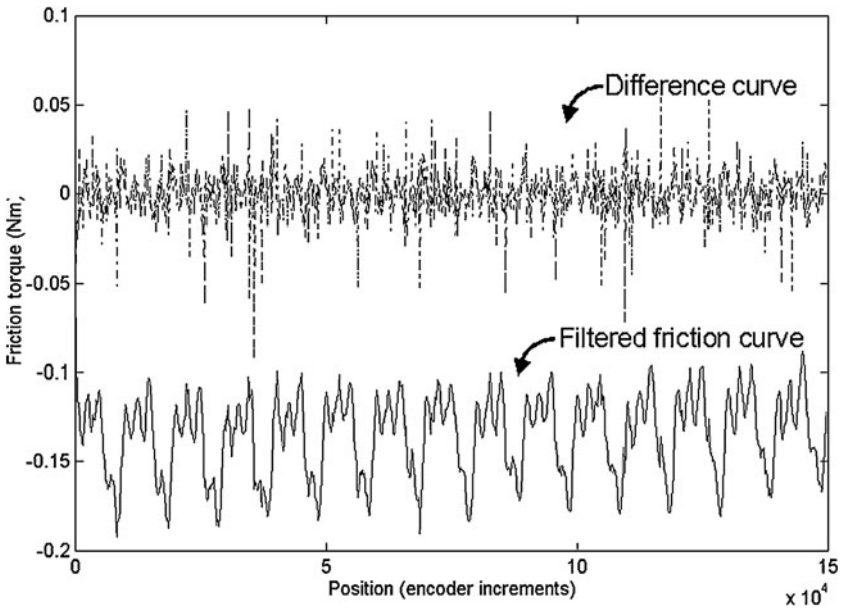

(b) Negative direction

Fig. 7 Filtered static friction curves

denote the angular acceleration of the motor shaft; τ_{m} represents the motor output torque; and τ_{f} indicates the friction torque. The equivalent inertia, J_a, is the combination of the motor inertia (the inertia of the rotor) and the load inertia (the compound inertia of the coupler, lead-screw bar, and worktable). The friction torque, τ_{f}, includes both the position-dependent friction, $\tau_{\mathrm{f}}^{\theta}$, and the velocity-dependent friction, $\tau_{\mathrm{f}}^{\omega}$. Therefore, Eq. 1 can be further rewritten as:

$$\tau_m - \left(\tau_{\mathrm{f}}^{\theta} + \tau_{\mathrm{f}}^{\omega}\right) = J_a\dot{\omega} = J_a\,\ddot{\theta}. \tag{2}$$

Assume that the velocity response of the tested feed drive servomechanism is maintained constant at ω_{s} during steady motions, i.e., $\omega = \omega_{\mathrm{s}}$ and $\dot{\omega} = 0$ at the steady state. Then, Eq. 2 can be rewritten as:

$$\tau_m - \left(\tau_{\mathrm{f}}^{\theta} + \tau_{\mathrm{f}}^{\omega}\right) = 0 \tag{3}$$

and thus,

$$\tau_m = \tau_{\mathrm{f}}^{\theta} + \tau_{\mathrm{f}}^{\omega} = \tau_f. \tag{4}$$

Therefore, the friction torque, τ_{f}, can be obtained by measuring the motor output torque, τ_{m}, during steady motions. By collecting τ_{f} and ω_{s} data through constant velocity experiments, a friction–velocity map is constructed to identify the velocity-dependent friction, $\tau_{\mathrm{f}}^{\omega}$. However, the measured

friction torque, τ_f, includes the position-dependent friction, τ_f^{θ}, which is mainly induced by position-dependent perturbations. In addition, the velocity response, ω_s, is also affected by the external disturbances and unmodeled dynamics of the tested feed drive servomechanism. Thus, the friction and velocity data values obtained by constant velocity experiments can deteriorate the friction–velocity map and thus affect the identification results for velocity-dependent friction. Therefore, a modified velocity feedback control structure was employed in constant velocity experiments to obtain raw friction and velocity data values, and a friction extraction method was newly developed in this study with a view to obtaining reliable friction and velocity data values for the identification of velocity-dependent friction.

In this study, the modified velocity feedback control structure shown in Fig. 4 was employed in constant velocity experiments to obtain raw friction and velocity data values during steady motions. Furthermore, the nominal plant of the built-in velocity control loop is obtained as:

$$G_n(s) = \frac{16978.09}{s^2 + 158.966s + 16978.09}. \tag{5}$$

Figure 8 shows the step responses of the built-in velocity control loop and the nominal plant, $G_n(s)$, with different velocity command levels. The experimental results show that the nominal plant in Eq. 5 provides a good approximation to the built-in velocity control loop. Moreover, the filter, $Q(s)$, in Fig. 4 is designed as a low-pass filter with a unity gain and a bandwidth of 15.92 Hz. Figure 9 shows the step responses of the velocity feedback control systems with and without a DOB. For the system without a DOB, the average value of the steady response is 5.1451 rad/s, and the variance value of the steady response is 1.4108×10^{-2} rad/s. However, for the system with a DOB, the average value of the steady response becomes 5.2356 rad/s, and the variance value of the steady response becomes 1.4750×10^{-3} rad/s. Thus, the modified velocity feedback control structure can provide more steady motions than that with the built-in velocity control structure.

Since the modified velocity feedback control structure provides steady motion with velocity response ω_s, i.e., $\dot{\omega}_s \cong 0$, the equation of motion in the steady state can be obtained as:

$$\tau_m - \left(\tau_f^{\theta} + \tau_f^{\omega_s}\right) = J_a\dot{\omega}_s \cong 0 \tag{6}$$

where $\tau_f^{\omega_s}$ denotes the velocity-dependent friction corresponding to the angular velocity, ω_s. In a case where the tested feed drive servomechanism is actuated by the motor output torques, τ_{m1} and τ_{m2}, the velocity response approaches ω_{s1} and ω_{s2} at the position, θ, corresponding to the motor output torques, τ_{m1} and τ_{m2}, respectively. Since the position-dependent friction, τ_f^{θ}, is invariant at position θ, Eq. 6 can be used to obtain the equation of motion at position θ with different motor output torques as:

$$\tau_{m1} - \tau_f^{\omega_{s1}} - \tau_f^{\theta} \cong 0 \tag{7}$$

and

$$\tau_{m2} - \tau_f^{\omega_{s2}} - \tau_f^{\theta} \cong 0 \tag{8}$$

where $\tau_f^{\omega_{s1}}$ and $\tau_f^{\omega_{s2}}$ denote the velocity-dependent frictions at position θ corresponding to the angular velocities ω_{s1} and

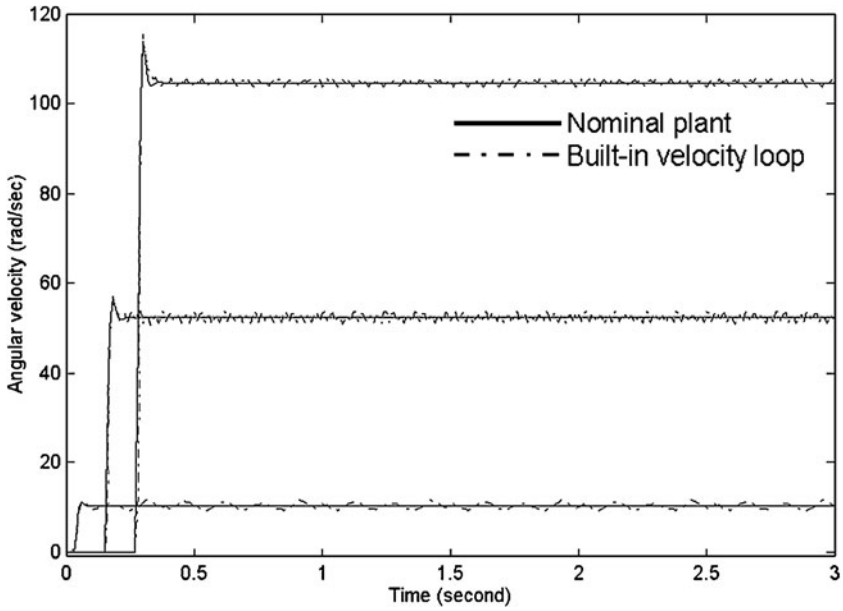

Fig. 8 Step responses of the built-in velocity control loop and the nominal plant

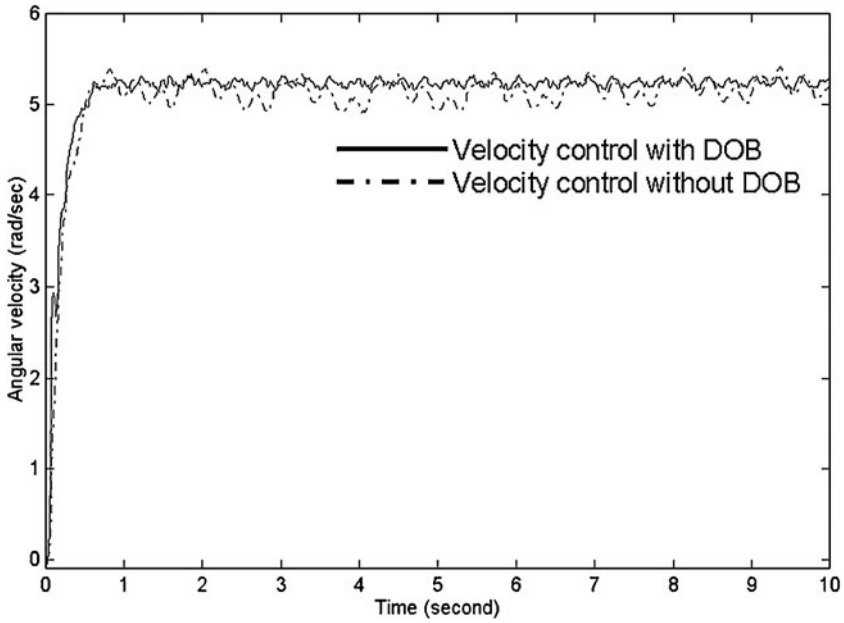

Fig. 9 Step responses of velocity control systems with and without DOB

ω_{s2}, respectively. By subtracting Eq. 7 from Eq. 8, the torque difference equation can be obtained as:

$$(\tau_{m2} - \tau_{m1}) - \left(\tau_f^{\omega_{s2}} - \tau_f^{\omega_{s1}}\right) \cong 0. \tag{9}$$

Thus, the position-dependent friction, τ_f^{θ}, is eliminated, and Eq. 9 is applied to identify the velocity-dependent friction, τ_f^{ω}. In this study, the static friction model described by Eq. 10 [21, 30, 31] is applied to describe the characteristics of the velocity-dependent friction of the tested feed drive servomechanism.

$$\tau_f^{\omega_s} = \left(\alpha_0 + \alpha_1 e^{-\left(\frac{\omega_s}{\omega_0}\right)^2}\right)\mathrm{sgn}(\omega_s) + \alpha_2\omega_s \tag{10}$$

where $(\alpha_0 + \alpha_1)$ represents the static friction, α_2 the viscous friction, and ω_0 the Stribeck velocity. Therefore, the friction difference, $\tau_f^{\omega_{s2}} - \tau_f^{\omega_{s1}}$, can be obtained as:

$$\begin{aligned}\tau_f^{\omega_{s2}} - \tau_f^{\omega_{s1}} &= \left[\left(\alpha_0 + \alpha_1 e^{-\left(\frac{\omega_{s2}}{\omega_0}\right)^2}\right)\mathrm{sgn}(\omega_{s2}) + \alpha_2\omega_{s2}\right] - \left[\left(\alpha_0 + \alpha_1 e^{-\left(\frac{\omega_{s1}}{\omega_0}\right)^2}\right)\mathrm{sgn}(\omega_{s1}) + \alpha_2\omega_{s1}\right] \\ &= \begin{cases} \alpha_1\left(e^{-\left(\frac{\omega_{s2}}{\omega_0}\right)^2} - e^{-\left(\frac{\omega_{s1}}{\omega_0}\right)^2}\right) + \alpha_2(\omega_{s2} - \omega_{s1}), \text{for } \omega_{s2} > 0 \text{ and } \omega_{s1} > 0 \\ \alpha_1\left[\left(-e^{-\left(\frac{\omega_{s2}}{\omega_0}\right)^2} - e^{-\left(\frac{\omega_{s1}}{\omega_0}\right)^2}\right)\right] + \alpha_2(\omega_{s2} - \omega_{s1}), \text{for } \omega_{s2} < 0 \text{ and } \omega_{s1} < 0 \end{cases}. \end{aligned} \tag{11}$$

Now, we substitute Eq. 11 into the torque difference equation, namely Eq. 9; then Eq. 9 becomes

$$(\tau_{m2} - \tau_{m1}) = \tau_f^{\omega_{s2}} - \tau_f^{\omega_{s1}} = \begin{cases} \alpha_1\left(e^{-\left(\frac{\omega_{s2}}{\omega_0}\right)^2} - e^{-\left(\frac{\omega_{s1}}{\omega_0}\right)^2}\right) + \alpha_2(\omega_{s2} - \omega_{s1}), \text{for } \omega_{s2} > 0 \text{ and } \omega_{s1} > 0 \\ \alpha_1\left[-\left(e^{-\left(\frac{\omega_{s2}}{\omega_0}\right)^2} - e^{-\left(\frac{\omega_{s1}}{\omega_0}\right)^2}\right)\right] + \alpha_2(\omega_{s2} - \omega_{s1}), \text{ for } \omega_{s2} < 0 \text{ and } \omega_{s1} < 0 \end{cases}. \tag{12}$$

In this study, we define data set (τ_{mb}, ω_{sb}), composed of motor output torque τ_{mb} and angular velocity ω_{sb} as the base data set, and data set (τ_{mj}, ω_{sj}), composed of motor output torque τ_{mj} and angular velocity ω_{sj}, as the target data set for $j = 1,\ldots,n$. Then, the torque difference equation, Eq. 12, can be rewritten as:

$$\left(\tau_{\mathrm{m}j}-\tau_{mb}\right)=\tau_{\mathrm{f}}^{\omega_{sj}}-\tau_{\mathrm{f}}^{\omega_{sb}}=\begin{cases}\alpha_1\left(e^{-\left(\frac{\omega_{sj}}{\omega_0}\right)^2}-e^{-\left(\frac{\omega_{sb}}{\omega_0}\right)^2}\right)+\alpha_2\left(\omega_{sj}-\omega_{\mathrm{s}b}\right), \text{for } \omega_{sj}>0 \text{ and } \omega_{sb}>0\\ \alpha_1\left[-\left(e^{-\left(\frac{\omega_{sj}}{\omega_0}\right)^2}-e^{-\left(\frac{\omega_{sb}}{\omega_0}\right)^2}\right)\right]+\alpha_2\left(\omega_{sj}-\omega_{sb}\right), \text{for } \omega_{sj}<0 \text{ and } \omega_{\mathrm{s}b}<0\end{cases} \quad \text{for} \quad j=1,\ldots,n. \tag{13}$$

Here, an optimization algorithm must be applied to compute the model parameters (α_1, α_2, ω_0) in order to minimize the estimation error, ε, as:

$$\varepsilon=\sqrt{\sum_{j=1}^{n}\left[\left(\tau_{\mathrm{m}j}-\tau_{mb}\right)-\left(\tau_{\mathrm{f}}^{\omega_{sj}}-\tau_{\mathrm{f}}^{\omega_{\mathrm{s}b}}\right)\right]^2}. \tag{14}$$

In this study, optimization function fminu provided by the Matlab optimization toolbox [32] is used to obtain the model parameters (α_1, α_2, ω_0). The velocity response ω_{sb} is the smallest velocity in the constant velocity experiments. Since ($\alpha_0 + \alpha_1$) represents static friction τ_e, parameter α_0 can be obtained as:

$$\alpha_0=\tau_e-\alpha_1 \tag{15}$$

where static friction τ_e is obtained from the friction compensation lookup tables as shown in Fig. 7 for a given angular position, θ. Therefore, by considering the asymmetry effect of friction [15], the velocity-dependent friction model is obtained as:

$$\hat{\tau}_{\mathrm{f}}^{\omega}=\begin{cases}\begin{cases}\alpha_0^{\mathrm{neg}}=-\tau_e^{neg}-\alpha_1^{\mathrm{neg}}\\ \left(\alpha_0^{\mathrm{neg}}+\alpha_1^{\mathrm{neg}}e^{-\left(\frac{\omega}{\omega_0^{\mathrm{neg}}}\right)^2}\right)\mathrm{sgn}(\omega)+\alpha_2^{\mathrm{neg}}\omega, \omega\le-\omega_{sb}^{neg}\end{cases}\\ \tau_e^{neg} \quad , -\omega_{sb}^{neg}<\omega<0\\ \tau_e^{pos} \quad , 0<\omega<\omega_{sb}^{pos}\\ \begin{cases}\alpha_0^{\mathrm{pos}}=\tau_e^{pos}-\alpha_1^{pos}\\ \left(\alpha_0^{pos}+\alpha_1^{pos}e^{-\left(\frac{\omega}{\omega_0^{\mathrm{pos}}}\right)^2}\right)\mathrm{sgn}(\omega)+\alpha_2^{pos}\omega, \omega\ge\omega_{sb}^{pos}\end{cases}\end{cases} \tag{16}$$

where τ_e^{neg} and τ_e^{pos} denote the static friction and ω_{sb}^{neg} and ω_{sb}^{pos} denote the base velocity responses for motion in the

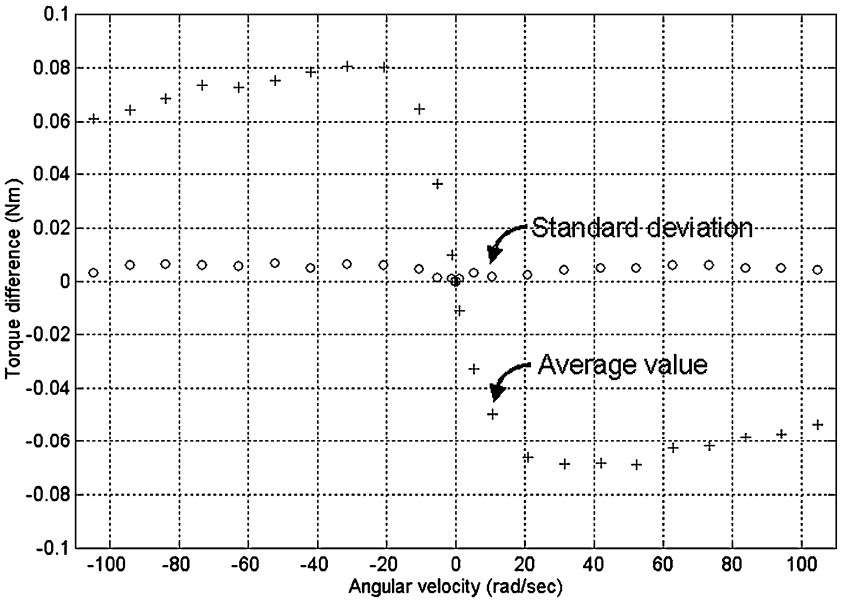

Fig. 10 Average values and the standard deviations of torque difference

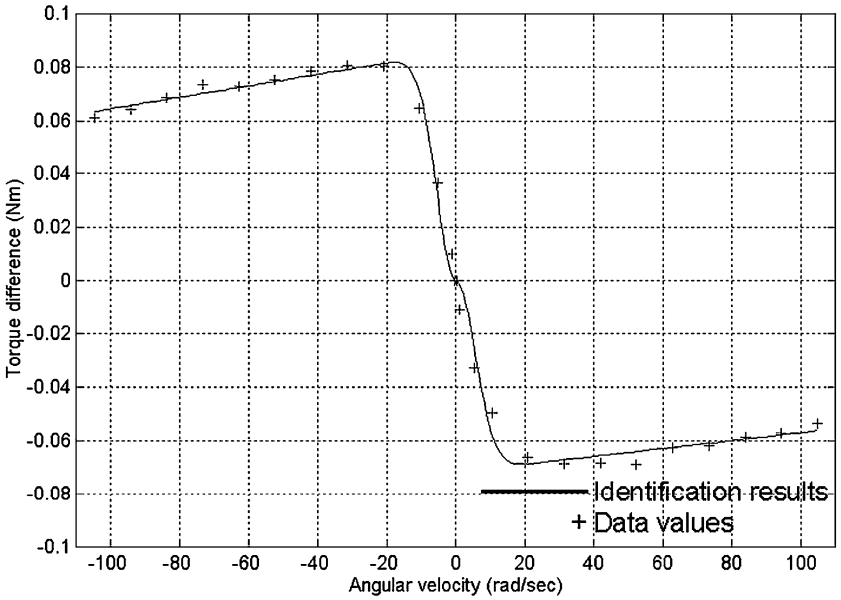

Fig. 11 Identification results for velocity-dependent friction

negative and positive directions, respectively. Coefficients $(\alpha_0^{neg}, \alpha_1^{neg}, \alpha_2^{neg}, \omega_0^{neg})$ represent the model parameters for motion in the negative direction and are different from coefficients $(\alpha_0^{pos}, \alpha_1^{pos}, \alpha_2^{pos}, \omega_0^{pos})$, which represent the model parameters for motion in the positive direction. Therefore, the procedure for identifying the velocity-dependent friction of a feed drive servomechanism is summarized as follows:

(a) Obtain the static friction, τ_e^{neg} and τ_e^{pos}, by performing the breakaway experiment described in Section 2.3.
(b) Obtain the base data sets, $(\tau_{mb}^{pos}, \omega_{sb}^{pos})$ and $(\tau_{mb}^{neg}, \omega_{sb}^{neg})$, and the target data sets, $(\tau_{mj}^{pos}, \omega_{sj}^{pos})$ and $(\tau_{mj}^{neg}, \omega_{sj}^{neg})$, for $j = 1,\ldots, n$, by performing the constant velocity experiment described in Section 2.4.
(c) Sort the obtained data by the angular position of the motor shaft, which ranges from the home position to the target position, as shown in Fig. 3.
(d) Compute torque difference $(\tau_{mj}^{pos} - \tau_{mb}^{pos})$ for $j = 1,\ldots, n$.
(e) Compute parameters $(\alpha_1^{pos}, \alpha_2^{pos}, \omega_0^{pos})$ by using an optimization algorithm.
(f) Compute torque difference $(\tau_{mj}^{neg} - \tau_{mb}^{neg})$ for $j = 1,\ldots, n$.
(g) Compute parameters $(\alpha_1^{neg}, \alpha_2^{neg}, \omega_0^{neg})$ by means of an optimization algorithm.
(h) Complete the velocity-dependent friction model as represented by Eq. 16.

Figure 10 shows the average values and standard deviations of the torque difference for different velocities; these were estimated using the data obtained from the constant velocity experiments. The standard deviations for all of the different velocities are lower than 10% of the corresponding average values. Figure 11 shows the identification results, and Table 3 lists the obtained parameters, $(\alpha_0^{pos}, \alpha_1^{pos}, \alpha_2^{pos}, \omega_0^{pos})$ and $(\alpha_0^{neg}, \alpha_1^{neg}, \alpha_2^{neg}, \omega_0^{neg})$.

4 Experimental results of sinusoidal motion tests

In this study, sinusoidal motion tests were carried out using the experimental setup in order to show the feasibility of the proposed friction identification method. Sinusoidal velocity command signals with an amplitude of 52.36 rad/s and frequencies of 0.5 and 1.0 Hz were used to perform the sinusoidal motion tests. The tracking errors are considered to evaluate the motion accuracy. For the evaluation of different identification methods, the feedforward friction compensation structure [1, 2], as

Table 3 Model parameters obtained using the approaches proposed in this study

Parameters for motion in the positive direction		Parameters for motion in the negative direction	
α_0^{pos}	$\tau_e^{pos} - \alpha_1^{pos}$ τ_e^{pos}: Fig. 7a	α_0^{neg}	$-\tau_e^{neg} - \alpha_1^{neg}$ τ_e^{neg}: Fig. 7b
α_1^{pos}	7.1662×10^{-2}	α_1^{neg}	8.5883×10^{-2}
α_2^{pos}	1.4802×10^{-4}	α_2^{neg}	2.1432×10^{-4}
ω_0^{pos}	7.93	ω_0^{neg}	7.65

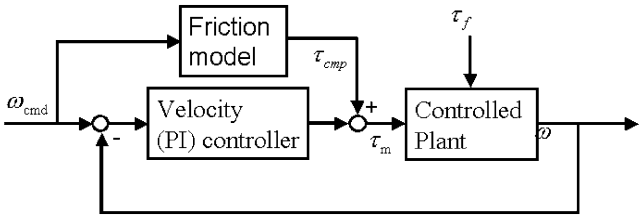

Fig. 12 Feedforward friction compensation and velocity feedback control

shown in Fig. 12, was used to control the motions of a feed drive servomechanism in the experimental setup. Here, the torque value for friction compensation, τ_{cmp}, is computed by referring to the velocity command, ω_{cmp}, and a friction model obtained by using different identification methods.

Figure 13 shows the friction–velocity map obtained by conventional approaches, and Table 4 lists the corresponding model parameters. Here, the friction model, as shown in Eq. 10, is adopted for the sake of comparison between different identification methods. Parameters α_1^{pos} and α_1^{neg} are further modified in order to consider the static friction, as shown in Figure 7. In Table 4, the values in brackets are the average values of α_0.

In this study, the sinusoidal motions obtained by applying different friction models are denoted as follows:

- UNCOMP: denotes the motion results obtained without using friction compensation.
- COMP_C: denotes the motion results obtained using the friction model parameters listed in Table 4.
- COMP_P: denotes the motion results obtained using the friction model parameters listed in Table 3.

Here, ten motions were adopted in each motion test to obtain the average motion performance. Furthermore, several performance indices were used to evaluate the steady motions in the motion tests, as follows:

- RMS: denotes the root mean square value of errors.
- MAX: denotes the maximum value of absolute errors.
- STD: denotes the standard deviation of data.

Figure 14 shows the experimental results of the sinusoidal motion tests, and Table 5 lists the statistical results for the obtained tracking errors. It is quite obvious that friction significantly deteriorates the motion accuracy when the velocity of the motion is near zero. Both of the MAX values exceed 10.0 rad/s for the motion tests. However, by applying friction compensation, the MAX values are reduced, with reductions of 24.16% and 34.11% achieved for the motion tests conducted using velocity command signals having frequencies of 0.5 and 1.0 Hz, respectively. In addition, RMS values of 26.97% and 44.16% were achieved for the different motion tests. Furthermore, the following two findings were made:

- The STD values for the motion test with the frequency of 0.5 Hz were generally larger than that for the motion test with the frequency of 1.0 Hz.
- The rate of reduction for the motion test with the frequency of 0.5 Hz was generally less than that for the motion test with the frequency of 1.0 Hz.

These observations follow from the fact that the friction compensation performance is usually limited for low-velocity motions because of (1) the difficulty in estimating

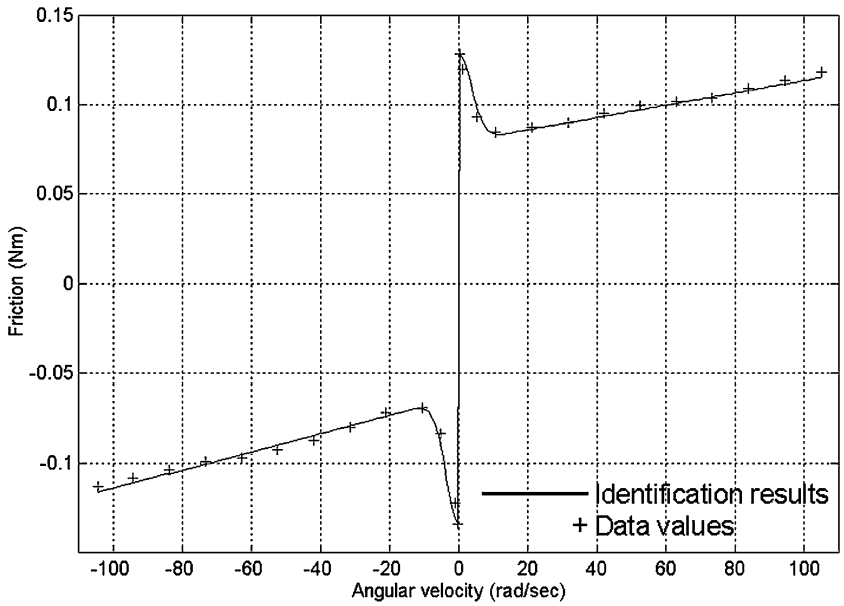

Fig. 13 The friction–velocity map and friction identification results

Table 4 Friction model parameters obtained by conventional approaches

Parameters for motion in the positive direction		Parameters for motion in the negative direction	
α_0^{pos}	$\tau_e^{pos} - \alpha_1^{pos}\left(7.9 \times 10^{-2}\right)$	α_0^{neg}	$-\tau_e^{neg} - \alpha_1^{neg}\left(6.3 \times 10^{-2}\right)$
α_1^{pos}	4.9660×10^{-2}	α_1^{neg}	7.0987×10^{-2}
α_2^{pos}	3.4532×10^{-4}	α_2^{neg}	5.1030×10^{-4}
ω_0^{pos}	5.2	ω_0^{neg}	5.1

friction characteristics at a low velocity and (2) the validity of the selected friction model at a low velocity. In comparison with a conventional identification method, the RMS values were further reduced and reductions of 9.52% and 6.24% were achieved in the experiments. The MAX value was slightly increased (by 0.99%) for the motion test with the frequency of 0.5 Hz, with the MAX value increased by 4.49% for the motion test with the frequency of 1.0 Hz. Thus, the increases in the MAX values could mainly be caused by the inertia effect induced by the motor inertia (the inertia of the rotor) and the load inertia (the compound inertia of the coupler, lead-screw bar, and worktable). However, the experimental results show that friction compensation can significantly improve the accuracy of feed drive servomechanism motions. Here, the STD values for the motion test with the frequency of 0.5 Hz are <1.5% of the corresponding average values, and the STD values for the motion test with the frequency of 1.0 Hz are

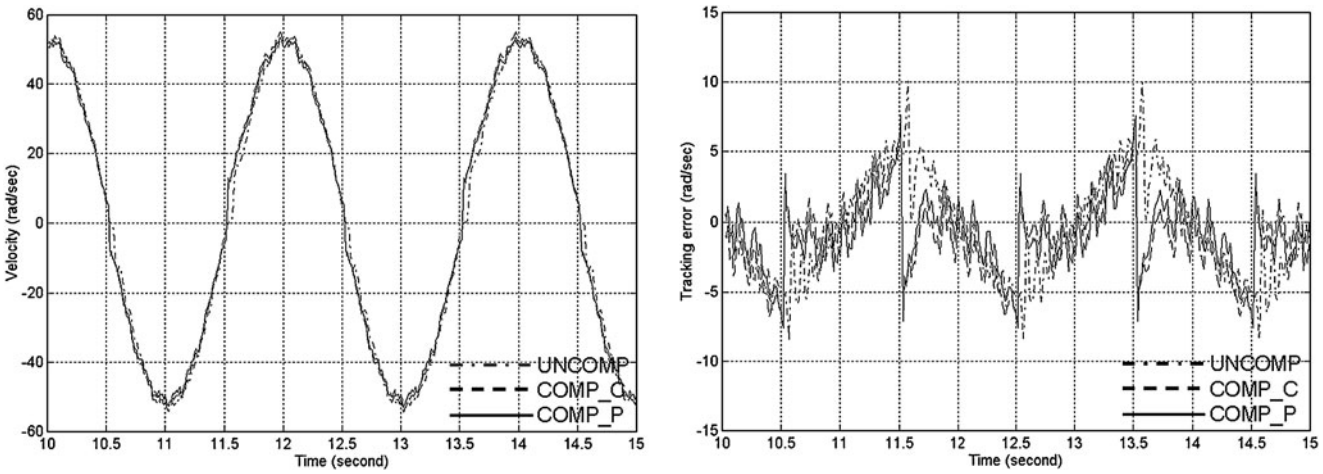

(a) Sinusoidal motions with a frequency of 0.5 Hz

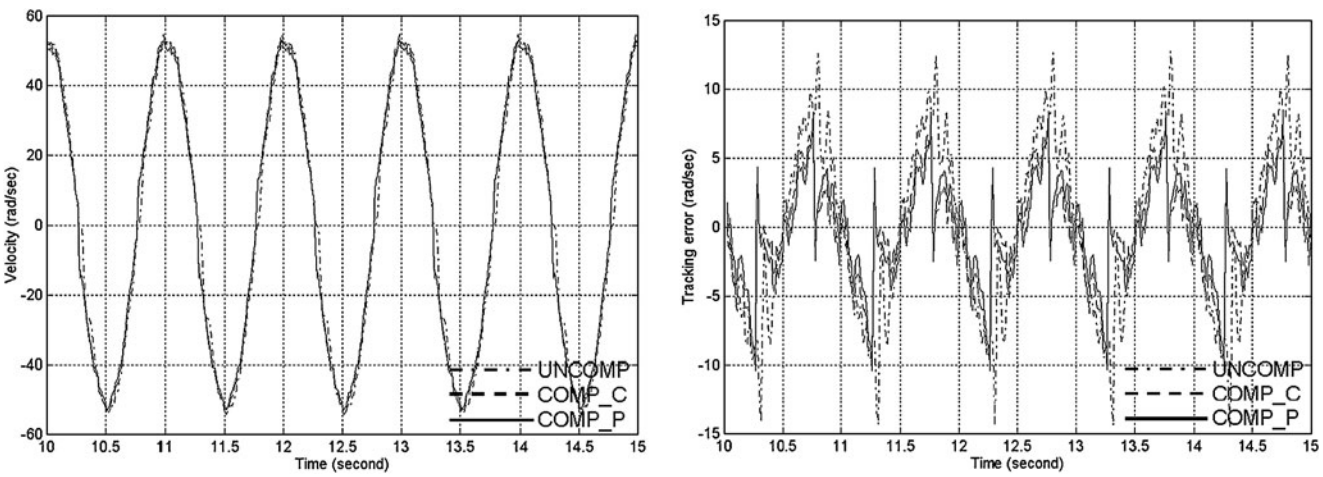

(b) Sinusoidal motions with a frequency of 1.0 Hz

Fig. 14 Experimental results of sinusoidal motion tests

Table 5 Statistical results for tracking errors in different motion tests

	0.5 Hz		1.0 Hz	
	RMS (rad/s) STD (%)	MAX (rad/s) STD (%)	RMS (rad/s) STD (%)	MAX (rad/s) STD (%)
UNCOMP	3.6264	10.0807	6.3411	12.7780
	0.18	0.26	0.21	0.53
COMP_C	2.9273	7.5704	3.7767	8.0580
	1.41	1.27	0.12	0.58
COMP_P	2.6485	7.6454	3.5410	8.4200
	1.43	1.25	0.16	0.63

<1.0% of the corresponding average values. Thus, the experimental results demonstrate the feasibility of the friction modeling method proposed in this study.

5 Conclusions

This study aimed at developing friction identification methods that consider the unavoidable effects induced by the position-dependent perturbations and unmodeled dynamics of the feed drive servomechanisms of CNC machine tools. In this study, a modified velocity control structure consisting of a built-in velocity control loop and a disturbance observer was developed to compensate for the speed perturbations induced by external disturbances and system uncertainties during constant velocity experiments. The experimental results showed that the modified velocity control structure could provide steady motions to the tested feed drive servomechanism in the steady state. The variance of the steady velocity response significantly reduced from 1.4108×10^{-2} to 1.4750×10^{-3} rad/s. Moreover, friction and velocity data were obtained through constant velocity experiments, and a friction extraction method was developed to remove position-dependent perturbations by considering the subtraction of different torque values. By applying the modified velocity control structure and the developed friction extraction method, more reliable friction and velocity data values could be obtained, which could be used to construct a friction model to reduce the uncertainties in the estimated friction characteristics. Furthermore, several experiments and motion tests were carried out on a three-axis CNC milling machine, and the feedforward friction compensation structure was applied to control the motions of a feed drive servomechanism of the CNC milling machine in order to evaluate different friction models obtained by different identification methods. The experimental results of these motion tests indicated that the friction-compensated motion control system with the friction model developed in this study reduced the RMS values of tracking errors by 44.16% (the best case) and 26.97% (the worse case). Moreover, the RMS values of tracking errors were found to be further reduced by 9.52% in the experiments, as compared to conventional methods. The experimental results thus demonstrated the feasibility of the proposed identification method for application to the motion control design of CNC machine tools.

In this study, a static friction model was used to describe the friction characteristics of a feed drive servomechanism. Many studies [3, 4, 8, 15] have reported that friction can exhibit characteristics such as the Dahl effect [33], friction lag [15], pre-sliding displacement [21], and stick-slip motion [34], which cannot be described by static friction models because of the internal dynamics of friction. Therefore, even though the experimental results showed that an improvement in the tracking accuracy was achieved by using the identification method proposed in this study, the motion performance could be further improved by considering the dynamic properties of friction.

Acknowledgments This project was supported by the Industrial Technology Research Institute, ROC, project number 8353CA3200, which was subcontracted from the Ministry of Economic Affairs, ROC. We would like to thank Mr. Jin-Tsu Sun (Mechanical and Systems Laboratories, Industrial Technology Research Institute, ROC) for the assistance in experiments and valuable comments.

References

1. Tsai MC, Chiu IF, Cheng MY (2004) Design and implementation of command and friction feedforward control for CNC motion controllers. IEE Proc Control Theory Appl 151(1):13–20
2. Elfizy AT, Bone GM, Elbestawi MA (2004) Model-based controller design for machine tool direct feed drives. Int J Mach Tools Manuf 44(5):465–477
3. Shih YT, Lee AC (2003) Survey on modeling and control for motion systems with friction. Journal of the Chinese Society of Mechanical Engineers, Transactions of the Chinese Institute of Engineers, Series C 24(4):337–352
4. Armstrong-Helouvry B, Dupont P, Canudas-de-Wit C (1994) A survey of models, analysis tools and compensation methods for the control of machines with friction. Automatica 30(7):1083–1138
5. Yeh SS, Tsai ZH, Hsu PL (2009) Applications of integrated motion controllers for precise CNC machines. Int J Adv Manuf Technol 44(9–10):906–920

6. Mei ZQ, Xue YC, Yang RQ (2006) Nonlinear friction compensation in mechatronic servo systems. Int J Adv Manuf Technol 30 (7–8):693–699
7. Chen JS, Kuo YH, Hsu WY (2006) The influence of friction on contouring accuracy of a Cartesian guided tripod machine tool. Int J Adv Manuf Technol 30(5–6):470–478
8. Awrejcewicz J, Olejnik P (2005) Analysis of dynamic systems with various friction laws. Appl Mech Rev 58(1–6):389–410
9. Chen CL, Jang MJ, Lin KC (2004) Modeling and high-precision control of a ball-screw-driven stage. Precis Eng 28(4):483–495
10. Persianoff R, Ray P, Vidal O (2003) Comparison between an experimental study and a numerical model of the dynamic behaviour of machine-tool slideways. Proc Inst Mech Eng B J Eng Manuf 217(8):1111–1115
11. Hsieh C, Pan YC (2000) Dynamic behavior and modelling of the pre-sliding static friction. Wear 242(1–2):1–17
12. Polycarpou AA, Soom A (1996) A two-component mixed friction model for a lubricated line contact. Journal of Tribology, Transactions of the ASME 118:183–189
13. Cetinkunt S, Yu WL, Filliben J, Donmez A (1994) Friction characterization experiments on a single point diamond turning machine tool. Int J Mach Tools Manuf 34(1):19–32
14. Marui E, Endo H (1992) Significance of contact resistance in boundary lubrication. Wear 156(1):49–55
15. Armstrong-Helouvry B (1991) Control of machines with friction. Kluwer, Boston
16. Armstrong BSR, Chen Q (2008) The Z-properties chart. IEEE Control Syst Mag 28(5):79–89
17. Cheok KC, Hu H, Loh NK (1988) Modeling and identification of a class of servomechanism systems with stick-slip friction. Journal of Dynamic Systems, Measurement and Control, Transactions of the ASME 110(3):324–328
18. Karnopp D (1985) Computer simulation of stick-slip friction in mechanical dynamic systems. Journal of Dynamic Systems, Measurement and Control, Transactions of the ASME 107 (1):100–103
19. Kim JH, Chae HK, Jeon JY, Lee SW (1996) Identification and control of systems with friction using accelerated evolutionary programming. IEEE Control Syst Mag 16(4):38–47
20. Canudas-de-Wit C, Lischinsky P (1997) Adaptive friction compensation with partially known dynamic friction model. Int J Adapt Control and Signal Process 11(1):65–80
21. Canudas-de-Wit C, Olsson H, Astrom KJ, Lischinsky P (1995) A new model for control of systems with friction. IEEE Trans Automat Contr 40(3):419–425
22. Popovic MR, Goldenberg AA (1998) Modeling of friction using spectral analysis. IEEE Trans Robot Autom 14(1):114–122
23. Ohnishi K (1987) A new servo method in mechatronics. Transactions of the Japan Society for Electrical Engineering 107(D):83–86
24. Matsushita Co. (2004) Panasonic MINAS A4-series instruction manual (DV0P4210). Matsushita Electric Industrial Co., Ltd
25. Söderström T, Stoica P (1989) System identification. Prentice Hall, New York
26. Choi BK, Choi CH, Lim K (1999) Model-based disturbance attenuation for CNC machining centers in cutting process. IEEE/ASME Trans Mechatron 4(2):157–168
27. Lee HS, Tomizuka M (1996) Robust motion controller design for high accuracy positioning systems. IEEE Transactions on Industrial Electronics 43:48–55
28. Umeno T, Hori Y (1991) Robust speed control of servomotors using modern two degrees-of-freedom controller design. IEEE Transactions on Industrial Electronics 38:363–368
29. Oppenheim AV, Schafer RW (1989) Discrete-time signal processing. Prentice Hall, New York
30. Garcia E, De-Santos PG, Canudas-de-Wit C (2002) Velocity dependence in the cyclic friction arising with gears. Int J Rob Res 21(9):761–771
31. Lischinsky P, Canudas-de-Wit C, Morel G (1999) Friction compensation for an industrial hydraulic robot. IEEE Control Syst Mag 19(1):25–32
32. Grace A (1994) Optimization toolbox for use with MATLAB, user's guide. The MathWorks Inc.
33. Dahl PR (1976) Solid friction damping of mechanical vibrations. AIAA J 14(12):1675–1682
34. Kato S, Yamaguchi K, Matsubayashi T (1974) Stick-slip motion of machine tool slideway. Journal of Engineering for Industry, Transactions of the ASME 96(2):557–566